Contribution from the Department of Chemistry,
University of Vermont, Burlington, Vermont 05405

# Stereodynamics of *trans*-[$(t\text{-}C_4H_9)_2PR]_2M(CO)X$ Systems (R = H, $CH_3$; M = Rh(I), Ir(I); X = Cl, Br, I). Assignment of Conformational Preferences and Conformational Exchange Itineraries

C. Hackett Bushweller,* Christopher D. Rithner,* and David J. Butcher

*Received October 7, 1985*

$^{31}P\{^1H\}$ and $^{13}C\{^1H\}$ dynamic NMR (DNMR) spectra of *trans*-$[(t\text{-}C_4H_9)_2PR]_2M(CO)X$ (R = H, $CH_3$; M = Rh(I), Ir(I); X = Cl, Br, I) show decoalescence phenomena that are assigned to slowing rotation about P–M and P–($t$-$C_4H_9$) bonds. Rotation about the P–M bonds is slow on the NMR chemical exchange time scale (rate constants less than 1 $s^{-1}$) at about 210 K ($\Delta G^{\ddagger}$ = 12–16 kcal/mol). *tert*-Butyl rotation is slow at about 140 K ($\Delta G^{\ddagger} \approx 7.5$ kcal/mol). $^{31}P\{^1H\}$ spectra at about 210 K (slow P–M rotation) show as many as three subspectra (three conformations). There is a dominant subspectrum at higher frequency (lower field), which is due to a conformation that has equivalent phosphorus atoms, and a second subspectrum with a lower population, which is due to a conformation with diastereotopic phosphorus atoms. Except for those complexes having R = H and X = I, there is a third, minor subspectrum at lower frequency (higher field), which is due to a conformation having equivalent phosphorus atoms. In conjunction with other evidence, the observed variations in subspectral populations as a function of halogen van der Waals radius provide circumstantial evidence for assigning the major subspectrum (equivalent phosphorus atoms) to a conformation having both R groups syn to halogen. The minor subspectrum (equivalent phosphorus atoms) is assigned to a conformation having both R groups syn to carbon monoxide. The subspectrum that shows diastereotopic phosphorus atoms is assigned to an anti conformation having one R group syn to halogen and the other syn to carbon monoxide. DNMR line-shape simulations reveal a preferred intramolecular exchange itinerary that involves rotation of one phosphine at a time about a P–M bond. $^{31}P$ and $^{13}C$ NMR chemical shift correlations with molecular geometry are also deduced.

## Introduction

In metal–phosphine complexes, it is now well-established that stereochemical nonrigidity is the rule and is rarely the exception.[1] Establishing trends in conformational preference in solution and determining barriers to conformational exchange could be important in understanding reaction regioselectivity and asymmetric induction.[2-4] In spite of this, there have been relatively few thorough, systematic studies of the stereodynamics of metal–phosphine complexes[5,6] or the free, uncomplexed phosphines.[7-9]

This paper concerns $^{31}P\{^1H\}$ and $^{13}C\{^1H\}$ dynamic NMR (DNMR) studies of the Ir(I) and Rh(I) complexes **1–12**. These are well-characterized, stable species that are not prone to decomposition during long-term DNMR studies and structurally simple enough to make conformational assignments tractable. Coordination at the metal is square planar ($dsp^2$) with the possibility of distortion due to steric crowding.[10,11] The two bulky phosphines in each complex are trans. $^{31}P\{^1H\}$ DNMR spectra, $^{13}C\{^1H\}$ DNMR spectra, interatomic distance calculations, and variation of the halide ligand allow a strong circumstantial case for conformational assignments that are different from those presumed previously.[5,6] $^{13}C\{^1H\}$ DNMR spectra also allow a measurement of *tert*-butyl rotation barriers.

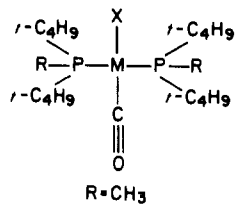


R = $CH_3$

1: M = Rh, X = Cl
2: M = Ir, X = Cl
3: M = Rh, X = Br
4: M = Rh, X = I
5: M = Ir, X = Br
6: M = Ir, X = I

R = H

7: M = Rh, X = Cl
8: M = Ir, X = Cl
9: M = Rh, X = Br
10: M = Ir, X = Br
11: M = Rh, X = I
12: M = Ir, X = I

## Results and Discussion

***trans*-[$(t\text{-}C_4H_9)_2PCH_3]_2Rh(CO)Cl$ (1).** The $^{31}P\{^1H\}$ NMR spectrum (101.2 MHz) of the rhodium complex **1** (0.04 M in toluene-$d_8$) at 360 K shows a broadened doublet at $\delta$ 42.2 ($^1J_{RhP}$ = 122 Hz).[12] The doublet results from scalar coupling of $^{31}P$ to $^{103}Rh$ ($I = {}^1/_2$; 100% natural abundance). Below 360 K, the spectrum decoalesces asymmetrically and, at 205 K, is separated into a series of well-resolved signals (Figure 1). A decomposition of the theoretical simulation of the 205 K spectrum (Figure 2) shows the $B_2$ portion of a $B_2X$ spin system (X = $^{103}Rh$; 59.9% of the total area of the composite spectrum), the AC part of an

(1) (a) Cotton, F. A. *Acc. Chem. Res.* **1968**, *1*, 257. (b) Muetterties, E. L. *Acc. Chem. Res.* **1970**, *3*, 266. (c) Beall, H.; Bushweller, C. H. *Chem. Rev.* **1973**, *73*, 465.
(2) (a) Morrison, J. D.; Masler, W. F.; Newburg, M. K. *Adv. Catal.* **1976**, *25*, 81. (b) Bosnich, B.; Fryzuk, M. D. *Top. Stereochem.* **1981**, *12*, 119. (c) Valentine, D., Jr.; Scott, J. W. *Synthesis* **1978**, 329. (d) Alyea, E. C., Meek, D. W., Eds. *Catalytic Aspects of Metal Phosphine Complexes*; Advances in Chemistry Series 196; American Chemical Society: Washington, DC, 1982. (e) Crabtree, R. *Acc. Chem. Res.* **1979**, *12*, 331. (f) Jardine, F. H. *Prog. Inorg. Chem.* **1981**, *28*, 63.
(3) Tolman, C. A. *Chem. Rev.* **1977**, *77*, 313.
(4) Halpern, J. *Inorg. Chim. Acta* **1981**, *50*, 11.
(5) (a) Bushweller, C. H.; Hoogasian, S.; English, A. D.; Miller, J. S.; Lourandos, M. Z. *Inorg. Chem.* **1981**, *20*, 3448. (b) Bushweller, C. H.; Rithner, C. D.; Butcher, D. J. *Inorg. Chem.* **1984**, *23*, 1967.
(6) (a) Mann, B. E.; Masters, C.; Shaw, B. L.; Stainbank, R. E. *J. Chem. Soc. D* **1971**, 1103. (b) Bright, A.; Mann, B. E.; Masters, C.; Shaw, B. L.; Slade, R. M.; Stainbank, R. E. *J. Chem. Soc. A* **1971**, 1826. (c) Mann, B. E.; Shaw, B. L.; Slade, R. M. *Ibid.* **1971**, 2976. (d) Empsall, H. D.; Hyde, E. M.; Mentzer, E.; Shaw, B. L. *J. Chem. Soc., Chem. Commun.* **1977**, 2285. (e) Smith, J. G.; Thompson, D. T. *J. Chem. Soc. A* **1967**, 1694. (f) Bennett, M. A.; Tomkins, I. B. *J. Organomet. Chem.* **1973**, *51*, 289. (g) Gill, D. F.; Mann, B. E.; Shaw, B. L. *J. Chem. Soc., Chem. Commun.* **1973**, 311. (h) Faller, J. W.; Johnson, B. V. *J. Organomet. Chem.* **1975**, *96*, 99. (i) Reed, C. A.; Roper, W. R. *J. Chem. Soc., Dalton Trans.* **1973**, 1365.
(7) (a) Bushweller, C. H.; Brunelle, J. A. *J. Am. Chem. Soc.* **1973**, *95*, 5949. (b) Brunelle, J. A.; Bushweller, C. H.; English, A. D. *J. Phys. Chem.* **1976**, *80*, 2598.
(8) (a) Bushweller, C. H.; Brunelle, J. A. *Tetrahedron Lett.* **1974**, 893. (b) Bushweller, C. H.; Lourandos, M. Z. *Inorg. Chem.* **1974**, *13*, 2514.
(9) (a) Rithner, C. D.; Bushweller, C. H. *J. Am. Chem. Soc.* **1985**, *107*, 7823.
(10) Empsall, H. D.; Mentzer, E.; Pawson, D.; Shaw, B. L. *J. Chem. Soc., Chem. Commun.* **1977**, 311.
(11) Hoffmann, P. R.; Yoshida, T.; Okano, T.; Otsuka, S.; Ibers, J. A. *Inorg. Chem.* **1976**, *15*, 2462.
(12) $^{31}P$ NMR chemical shifts are calibrated relative to trimethyl phosphite in a pertinent solvent, which is sealed in a coaxial reference tube. The $^{31}P$ chemical shift of 85% $H_3PO_4$ is 142.1 ppm lower frequency (higher field) from trimethyl phosphite in toluene-$d_8$ at 310 K and 142.8 ppm lower frequency from trimethyl phosphite in 33% $CD_2Cl_2$/33% $CF_2ClH$/33% $CFCl_2H$ at 310 K.

0020-1669/86/1325-1610$01.50/0 

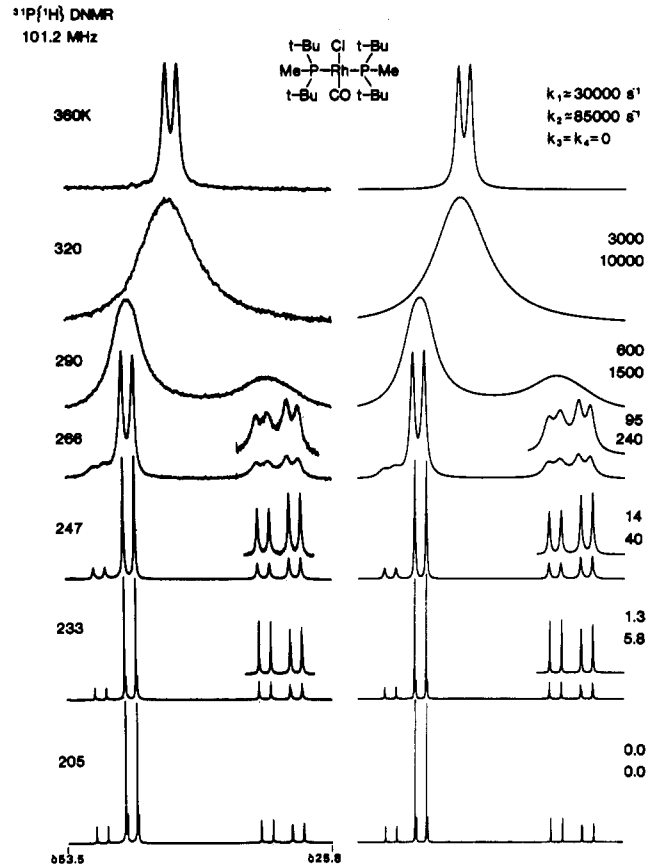


**Figure 1.** $^{31}P\{^1H\}$ DNMR spectra of *trans*-$[(t\text{-}C_4H_9)_2PCH_3]_2Rh(CO)Cl$ (**1**). Rate constants for theoretical simulations are defined in eq 1 and 2.

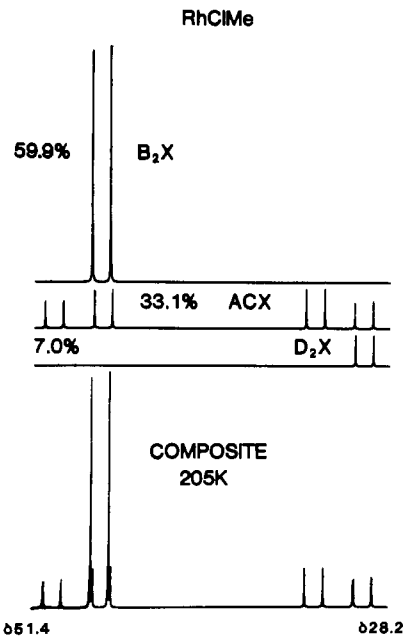


**Figure 2.** Decomposition of the $^{31}P\{^1H\}$ NMR spectrum of **1** at 205 K.

ACX spin system (33.1%), and the $D_2$ portion of a $D_2X$ spin system (7.0%).[13] The minor $D_2X$ doublet and the outer doublet of the C resonance almost superimpose (Figure 2). NMR parameters and subspectral populations are compiled in Table I.

(13) The computer program DNMR4 was used to simulate these static NMR line shapes and all the exchange-broadened DNMR spectra in this report: Bushweller, C. H.; Letendre, L. J.; Brunelle, J. A.; Bilofsky, H. S.; Whalon, M. R.; Fleischman, S. H. Quantum Chemistry Program Exchange, Indiana University, 1983; Program 466.

**Table I.** $^{31}P$ NMR Parameters and Subspectral Populations for Complexes **1–12** under Conditions of Slow Rotation about Metal–Phosphorus Bonds

| compd | spin syst obsd at slow exchange[a] | $^{31}P$ NMR chem shifts, ppm | $^1J_{RhP}$, Hz | $^2J_{PP}$, Hz | rel population (temp, K) |
|---|---|---|---|---|---|
| **1**[b] | $B_2X$ | 47.1 | 119.3 | | 0.599 (205) |
| | $D_2X$ | 29.8 | 121.0 | | 0.070 |
| | ACX | 48.4 | 118.2 | 323.0 | 0.331 |
| | | 31.6 | 123.1 | 323.0 | |
| **2**[b] | $B_2$ | 33.7 | | | 0.607 (214) |
| | $D_2$ | 18.5 | | | 0.063 |
| | AC | 36.1 | | 319.2 | 0.330 |
| | | 19.1 | | 319.2 | |
| **3**[b] | $B_2X$ | 39.7 | 117.2 | | 0.666 (214) |
| | $D_2X$ | 23.7 | 119.7 | | 0.034 |
| | ACX | 40.8 | 117.2 | 319.2 | 0.300 |
| | | 26.1 | 120.8 | 319.2 | |
| **4**[b] | $B_2X$ | 39.7 | 116.2 | | 0.838 (223) |
| | $D_2X$ | 26.8 | 118.0 | | 0.006 |
| | ACX | 40.7 | 115.4 | 311.0 | 0.156 |
| | | 29.7 | 119.2 | 311.0 | |
| **5**[b] | $B_2$ | 33.4 | | | 0.705 (214) |
| | $D_2$ | 19.4 | | | 0.032 |
| | AC | 35.4 | | 311.9 | 0.263 |
| | | 20.7 | | 311.9 | |
| **6**[b] | $B_2$ | 28.1 | | | 0.845 (223) |
| | $D_2$ | 16.7 | | | 0.006 |
| | AC | 29.4 | | 304.2 | 0.149 |
| | | 19.2 | | 304.2 | |
| **7**[c] | $B_2X$ | 80.5 | 114.6 | | 0.782 (220) |
| | $D_2X$ | 40.8 | 118.1 | | 0.010 |
| | ACX | 85.1 | 116.2 | 320.7 | 0.208 |
| | | 45.0 | 116.6 | 320.7 | |
| **8**[d] | $B_2$ | 74.2 | | | 0.900 (223) |
| | $D_2$ | 34.2 | | | 0.002 |
| | AC | 80.3 | | 315.7 | 0.098 |
| | | 37.2 | | 315.7 | |
| **9**[d] | $B_2X$ | 76.9 | 112.3 | | 0.851 (214) |
| | $D_2X$ | 37.5 | 116.0 | | 0.003 |
| | ACX | 83.2 | 113.5 | 315.5 | 0.146 |
| | | 42.7 | 114.8 | 315.5 | |
| **10**[d] | $B_2$ | 72.5 | | | 0.946 (214) |
| | $D_2$ | 33.0 | | | 0.001 |
| | AC | 80.6 | | 309.7 | 0.053 |
| | | 35.8 | | 309.7 | |
| **11**[d] | $B_2X$ | 72.3 | 109.9 | | 0.935 (214) |
| | ACX | 81.0 | 112.3 | 310.1 | 0.065 |
| | | 43.0 | 112.7 | 310.1 | |
| **12**[d] | $B_2$ | 67.2 | | | 0.975 (214) |
| | AC | 77.8 | | 301.5 | 0.025 |
| | | 33.5 | | 301.5 | |

[a] X = $^{103}Rh$ ($I = {}^1/_2$). [b] Solvent toluene-$d_8$. [c] Solvent 20% $CDCl_3$/80% toluene-$d_8$. [d] Solvent $CDCl_3$.

Below 205 K, the $^{31}P\{^1H\}$ spectrum of **1** (0.04 M in 33% $CD_2Cl_2$/33% $CFCl_2H$/33% $CF_2ClH$) shows changes in subspectral populations but *no additional decoalescence phenomena* down to 125 K.

The DNMR spectra in Figure 1 might reflect *inter*molecular or *intra*molecular exchange processes. It is necessary to distinguish between the two possibilities. For all of the Rh(I) complexes in this study, $^{103}Rh$–$^{31}P$ scalar coupling ($^1J_{RhP}$ = 110–122 Hz; Table I) is observed at room temperature *and above*. The addition of free phosphine to the NMR sample causes no coalescence of $^{31}P\{^1H\}$ NMR signals for free and bound phosphine and causes no change in the $^{31}P\{^1H\}$ DNMR spectra of **1**. From both of these observations, it must be concluded that Rh–P bond dissociation (or *inter*molecular phosphine exchange) does not occur even at a slow rate on the NMR chemical exchange time scale at temperatures as high as 360 K (Figure 1). The $^{13}C\{^1H\}$ NMR spectrum of the carbon monoxide ligand of **1** at 310 K shows both $^{103}Rh$–$^{13}C$ ($^1J_{RhC}$ = 74 Hz) and $^{31}P$–$^{13}C$ ($^2J_{PC}$ = 16 Hz) scalar coupling which reveals no metal–carbon monoxide dissociation. Removal or exchange of chloride in complexes such as **1** requires the use of a Lewis acid or excess ionic halide *in polar solvents*.[6i]

**Table II.** $^{13}C$ NMR Chemical Shifts for Complexes **1** and **2** under Conditions of Slow Rotation about Metal–Phosphorus Bonds

| compd (temp, K) | $*C(CH_3)_3$ ($^vJ_{PC}$, Hz) | $C(*CH_3)_3$ | $PCH_3$ ($^vJ_{PC}$, Hz) | CO |
|---|---|---|---|---|
| **1** (205 K)[a] | 34.7 (t, 20)[b] | 29.4 | 4.12 (t, 22.8) | 189.7 (m) |
| | 35.5 (m)[c] | 29.7 | 8.17 (t, 22.0) | |
| | | | 2.84 (d, 21.7)[d] | |
| | | | 7.66 (d, 22.8) | |
| **2** (214 K)[a] | 35.4 (t, 26) | 29.3 | 2.40 (t, 29.6) | 173.5 (m) |
| | | 29.8 | 8.00 (t, 26.0) | |
| | | | 0.98 (d, 27.7) | |
| | | | 7.38 (d, 29.6) | |

[a] Solvent $CDCl_3$. [b] t = triplet. [c] m = multiplet. [d] d = doublet.

In the *nonpolar* solvents used in our DNMR studies and in the absence of Lewis acids or ionic halides, metal–chloride dissociation does not occur. Thus, for spectroscopic and chemical reasons, it must be concluded that the rate process observed in Figure 1 is intramolecular and involves conformational exchange among at least three species, which give the $B_2X$, $D_2X$, and ACX subspectra. It is important to note that the $^2J_{PP}$ value (323 Hz; Table I) for the diastereotopic phosphorus atoms that give the ACX subspectrum verifies that the two phosphines are trans and not cis.[14] The $^2J_{PP}$ value for cis phosphines is usually much smaller in magnitude.[14]

The $^{13}C\{^1H\}$ NMR spectrum (62.9 MHz) of **1** (0.04 M in $CDCl_3$) at 303 K shows signals at $\delta$ 189.4 (CO; $^1J_{RhC}$ = 74 Hz, $^2J_{PC}$ = 16 Hz), $\delta$ 35.0 ($t$-$C_4H_9$ quaternary; $^vJ_{PC}$ = 17.6 Hz), and $\delta$ 29.7 ($t$-$C_4H_9$ methyls; $^vJ_{PC}$ = 5.2 Hz) and an *exchange-broadened* resonance at $\delta$ 5.1 ($PCH_3$). Part of the spectrum at 303 K is shown in Figure 3. $^{13}C\{^1H\}$ NMR parameters are compiled in Table II.

Below 303 K, the quaternary carbon, *tert*-butyl methyl and *P*-methyl resonances all decoalesce and give sharp signals at 214 K (Figure 3). In particular, the *P*-methyl resonance is separated at 214 K into four signals including a dominant virtual triplet, a minor virtual triplet, and two doublets of equal area, which are marked respectively with a solid circle, an ×, and open circles in Figure 3. From systematic calculations of a series of four-spin spectra,[15] the virtual triplet pattern for the dominant signal at $\delta$ 4.12 ($^vJ_{PC}$ = 22.8 Hz) is consistent with a $^{13}CPRhP'$ system that has *equivalent* phosphorus atoms. It corresponds to the dominant $B_2X$ doublet in the $^{31}P\{^1H\}$ spectrum at 205 K (Figure 2). The minor triplet at $\delta$ 8.17 ($^vJ_{PC}$ = 22 Hz) labeled with an × in Figure 3 is also consistent with equivalent phosphorus atoms and corresponds to the minor $D_2X$ subspectrum in the $^{31}P\{^1H\}$ spectrum. The doublets at $\delta$ 7.66 ($^vJ_{PC}$ = 22.8 Hz) and $\delta$ 2.84 ($^vJ_{PC}$ = 21.7 Hz) labeled with open circles in Figure 3 result from a $^{13}CPRhP'$ spin system that has *different* chemical shifts for the two phosphorus atoms. Thus, the two $^{13}C\{^1H\}$ doublets of equal area at $\delta$ 7.66 and 2.84 correspond directly to the $^{31}P\{^1H\}$ ACX subspectrum (Figure 2), which clearly shows diastereotopic phosphorus atoms.

The quaternary carbon resonance decoalesces below 303 K and is separated at 214 K into a dominant virtual triplet at $\delta$ 34.7 ($^vJ_{PC}$ = 20 Hz; see solid circle in Figure 3), indicating equivalent phosphorus atoms, and a multiplet centered at $\delta$ 35.5 (open circle). The chemical shift differences are quite small, and the spectrum has limited value. The *tert*-butyl methyl signal is decoalesced at 214 K into a dominant signal at $\delta$ 29.4 (solid circle) and a smaller signal at $\delta$ 29.7 (open circle), which are also very closely spaced and have limited informational content.

Below 214 K (Figure 3), the quaternary carbon and *P*-methyl carbon resonances (67.9 MHz) of **1** (0.04 M in 33% $CD_2Cl_2$/33% $CFCl_2H$/33% $CF_2ClH$) undergo no further decoalescence. The dominant *P*-methyl and quaternary carbon triplets do become

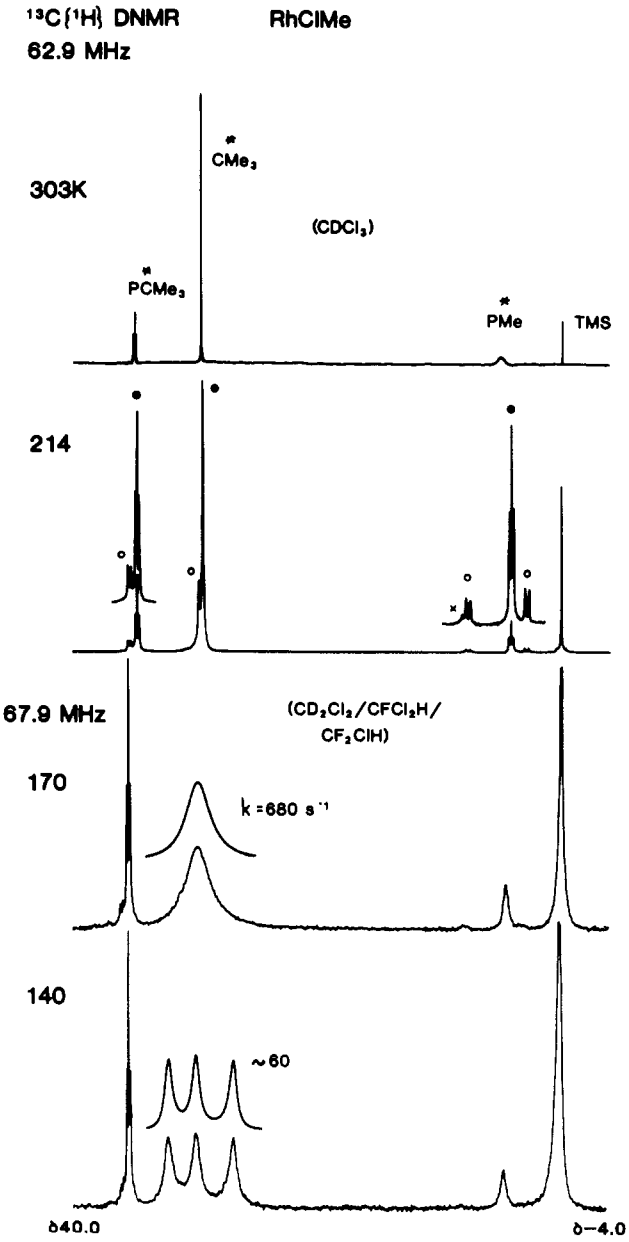


**Figure 3.** $^{13}C\{^1H\}$ DNMR spectra of *trans*-$[(t\text{-}C_4H_9)_2PCH_3]_2Rh(CO)Cl$ (**1**). The spectra at 303 and 214 K were run in $CDCl_3$ and, at 170 and 140 K, in $CD_2Cl_2/CFCl_2H/CF_2ClH$.

more dominant at lower temperatures. In addition, the $^{31}P\{^1H\}$ spectrum undergoes no further decoalescence down to 125 K. However, the $^{13}C\{^1H\}$ spectrum of the *tert*-butyl methyl groups undergoes a clear-cut decoalescence and, at 140 K, is separated into three broad singlets of equal *area* at $\delta$ 26.6, 29.7 and 32.0 (Figure 3). In light of the local symmetry proximate to a *tert*-butyl group (**13a**) and the observation of three *tert*-butyl methyl signals

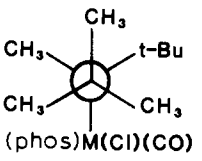


**13a**: M=Rh

**13b**: M=Ir

of *equal* area at 140 K, we are compelled to assign this decoalescence to threefold *tert*-butyl rotation. Threefold *tert*-butyl rotation does not effect any net change in molecular geometry and therefore will have no effect on the *tert*-butyl quaternary and *P*-methyl $^{13}C\{^1H\}$ resonances or on the $^{31}P\{^1H\}$ resonances of **1**.[16]

(14) For a review, see: Diehl, P., Fluck, E., Kosfeld, R., Eds. *NMR Basic Principles and Progress* Springer-Verlag: New York, 1979.

(15) The computer program UEAITR was used for simulating *static* spectra with four or more spins: Johannesen, R. B.; Ferretti, J. A.; Harris, R. K. Quantum Chemistry Program Exchange, Indiana University, 1979; Program 188.

A three-site DNMR simulation at 170 K gives a *tert*-butyl rotation barrier ($\Delta G^*$) of 7.6 ± 0.4 kcal/mol.[13] It is interesting to note that the rather large Rh(phos)(CO)Cl moiety raises the *tert*-butyl rotation barrier only 1.4 kcal/mol above that in the free, uncomplexed di-*tert*-butylmethylphosphine ($\Delta G^* = 6.2 \pm 0.3$ kcal/mol at 120 K).[9]

*Therefore, we assign the higher temperature decoalescence for* **1** *(Figure 1 and 3) to rotation about Rh–P bonds* ($\Delta G^* \approx 13$ *kcal/mol) and the lower temperature decoalescence (Figure 3) to tert-butyl rotation* ($\Delta G^* = 7.6$ *kcal/mol*). The three different $^{31}P\{^1H\}$ subspectra ($B_2X$, ACX, $D_2X$) observed at 205 K (Figure 2) correspond to three different equilibrium conformations associated with restricted rotation about the Rh–P bonds.

***trans*-[$(t$-$C_4H_9)_2PCH_3]_2Ir(CO)Cl$ (2).** The $^{31}P\{^1H\}$ NMR spectrum (101.2 MHz) of the iridium complex **2** (0.04 M in toluene-$d_8$) at 360 K is a broad *singlet* at $\delta$ 29.4.[12] Although $^{191}Ir$ (37.3% natural abundance) and $^{193}Ir$ (62.7% natural abundance) both have a spin of $^3/_2$, efficient nuclear quadrupolar relaxation decouples iridium from phosphorus in **2** and in all the other iridium complexes in this study. Below 360 K, the spectrum decoalesces and, at 214 K, is separated into a $B_2$ singlet (60.7%; equivalent phosphorus atoms), a smaller $D_2$ singlet (6.3%; equivalent phosphorus atoms), and an AC subspectrum (33.0%; $^2J_{PP} = 319$ Hz; diastereotopic and trans phosphorus atoms) as shown in Figures 4 and 5 (supplementary material). NMR parameters are compiled in Table I.

The $^{31}P\{^1H\}$ spectrum of **2** (0.03 M in 33% $CD_2Cl_2$/33% $CF_2ClH$/33% $CFCl_2H$) shows no additional decoalescence down to 130 K.

The $^{13}C\{^1H\}$ DNMR spectra of **2** are shown in Figure 6 (supplementary material). The spectrum of **2** at 305 K (0.03 M in $CDCl_3$) shows resonances at $\delta$ 173.5 (CO; $^2J_{PC} = 9$ Hz), $\delta$ 35.6 ($t$-$C_4H_9$ quaternary; $^vJ_{PC} = 25.0$ Hz), and $\delta$ 29.7 ($t$-$C_4H_9$ methyls) and an *exchange-broadened* peak at $\delta$ 3.1 ($PCH_3$). The observation of scalar coupling between the carbon monoxide carbon-13 and the phosphorus atoms reveals no carbon monoxide or phosphine dissociation at 305 K. In the relatively nonpolar $CDCl_3$, chloride dissociation also should not occur (vide supra). Between 305 and 214 K, the spectrum of **2** (Figure 6) decoalesces in a manner that is essentially identical with that for **1** (Figure 3). Although the signals for **2** are shifted slightly upfield as compared to those for **1**, the *P*-methyl group of **2** at 214 K gives a dominant virtual triplet ($\delta$ 2.4; $^vJ_{PC} = 29.6$ Hz; equivalent phosphorus atoms), a minor virtual triplet ($\delta$ 8.0; $^vJ_{PC} = 26.0$ Hz), and two doublets of *equal area* at $\delta$ 7.38 ($^vJ_{PC} = 29.6$ Hz) and $\delta$ 0.98 ($^vJ_{PC} = 27.7$ Hz), which reveal diastereotopic phosphorus atoms. The *tert*-butyl quaternary and methyl resonances also decoalesce into groups of very closely spaced signals (Table II). The *P*-methyl $^{13}C\{^1H\}$ spectrum of **2** at 214 K correlates precisely with the $^{31}P\{^1H\}$ spectrum at 214 K. The decoalescence phenomena that occur in the $^{31}P\{^1H\}$ and $^{13}C\{^1H\}$ spectra above 214 K are assigned to slowing rotation about the Ir–P bonds ($\Delta G^* \approx 14$ kcal/mol). Only the *tert*-butyl methyl $^{13}C\{^1H\}$ resonance of **2** (0.03 M in 33% $CD_2Cl_2$/33% $CFCl_2H$/33% $CF_2ClH$) decoalesces below 214 K and is separated at 130 K into three singlets or *equal area* at $\delta$ 27.0, 29.5, and 32.2 (Figure 6; Table II). This decoalescence is attributed to *tert*-butyl rotation (see **13b**; $\Delta G^* = 7.2 \pm 0.4$ kcal/mol at 160 K).

**Assignment of Conformational Preferences.** The three subspectra observed in the $^{31}P\{^1H\}$ spectra of **1** and **2** at about 210 K must be due to different molecular conformations associated with restricted rotation about the metal–phosphorus bonds. Assignments are problematical because NMR parameters that probe molecular geometry unequivocally (e.g., a Karplus relationship) are not available. Thus, we will present below a circumstantial case for conformational assignments that is based on observed variations of subspectral populations as a function of halogen steric bulk and other considerations.

One premise to be used in predicting equilibrium conformations in these systems has much precedent. The *tert*-butyl group is sterically large and will prefer to stagger and not eclipse the chlorine and carbon monoxide ligands. Staggering by *tert*-butyl groups is observed in the crystal structures of *trans*-[($t$-$C_4H_9)_2PC_6H_5]_2Rh(N_2)H$[11] and the cyclic *trans*-[$(t$-$C_4H_9)_2PC{\equiv}C(CH_2)_5C{\equiv}CP(t$-$C_4H_9)_2$]Ir(CO)Cl.[10] Conformations such as **14** ($t$-$C_4H_9$/Cl elipsing) and **15** ($t$-$C_4H_9$/CO eclipsing) are predicted to be unstable. A conformation such as **16** in which the P-methyl bond is in a plane perpendicular to the metal coordination plane and the *tert*-butyl groups are skewed only slightly away from perfect eclipsing also involves severe $t$-$C_4H_9$/Cl *and* $t$-$C_4H_9$/CO nonbonded repulsions. Thus, **16** is also predicted to be unstable. An example of a stable conformation with optimally staggered *tert*-butyl groups is **17**, which has both *P*-methyl groups syn to chlorine. A requirement of optimized staggering for a ($t$-$C_4H_9)_2P$ moiety about the Cl–M–CO axis then requires an eclipsing of the *P*-methyl groups by chlorine or carbon monoxide.

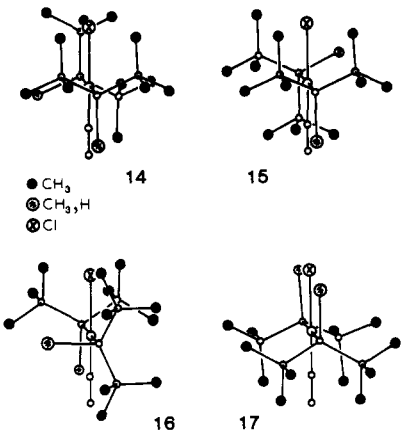


Therefore, we predict four equilibrium conformations for **1** and **2**, which are illustrated in eq 1: two diastereomeric syn forms (**17**, **18**) and two equivalent anti forms (**19**, **20**). A complete accounting of all the stable conformations of **1** or **2** must include *two* equivalent anti forms, which are interconverted directly by two simultaneous 180° rotations of both phosphines about the P–M bonds. There is a statistical preference of 2 for the anti forms over either one of the syn forms. In addition, an accurate kinetic model for conformational exchange to be used in any DNMR simulations must include two anti forms (vide infra).

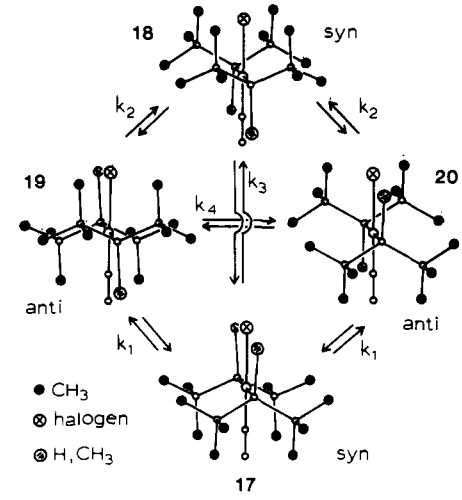


(1)

In the $^{31}P\{^1H\}$ and $^{13}C\{^1H\}$ spectra of **1** and **2** at about 210 K, which show slow rotation about the metal–phosphorus bonds,

(16) It is inevitable in these complexes that twisting away from perfect staggering about P–($t$-$C_4H_9$) bonds will occur in the equilibrium conformations.[9] This introduces rate processes involving low-torsion *tert*-butyl *libration* (or twisting) as well as threefold *tert*-butyl *rotation*. Libration does not involve vicinal eclipsings in the transition state and consistently has a much lower barrier than threefold *tert*-butyl rotation.[9] It is apparent that, at 140 K, *tert*-butyl rotation is slow while libration is fast. In fact, slow *tert*-butyl rotation *and* slow libration would give, in principle, *six tert*-butyl methyl resonances for a given phosphine moiety.

**Table III.** Cone Angles[a] and van der Waals Radii

| group | cone angle, deg | van der Waals radius, Å | group | cone angle, deg | van der Waals radius, Å |
|---|---|---|---|---|---|
| H | 75 | 1.2 | Cl | 102 | 1.8 |
| CO | 95 | 1.4[b] | Br | 105 | 2.0 |
| $CH_3$ | 90 | 2.0 | I | 107 | 2.2 |

[a] Reference 3. [b] Reference 17.

assignment of the anti resonances is trivial. In an anti form, the two phosphorus atoms are diastereotopic and will give anisochronous $^{31}P$ chemical shifts. Thus, the ACX subspectrum for **1** and the AC subspectrum for **2** are assigned to anti conformers **19** and **20** (eq 1). Likewise, the two *P*-methyl groups in an anti form are diastereotopic. The two *P*-methyl doublets of equal area observed in each of the 214 K $^{13}C\{^1H\}$ spectra for **1** and **2** are assigned to the anti forms.

Assignment of syn forms is more equivocal. The relative stabilities of the two syn forms (**17**, **18**; eq 1) will be determined by the relative sizes of halogen and carbon monoxide. In addition, the syn conformational preference will be determined by the relative degrees of crowding at the position syn to the two methyl groups (site 1 in structure **21a**) and the position gauche to the

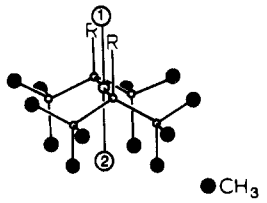


**21a:** R=$CH_3$
**21b:** R=H

four *tert*-butyl groups (site 2 in **21a**). The *larger* ligand will prefer to occupy the *less crowded* of sites 1 and 2 in **21a**. With use of both van der Waals radii and cone angle values for carbon monoxide (1.4 Å; 95°) and chlorine (1.94 Å; 102°), chlorine is determined to be the larger ligand (Table III).[3,17]

Interatomic distance calculations for **1** and **2** were done by using the computer program COORD.[19] An idealized geometry with standard bond lengths, perfect $C_{2v}$ symmetry, tetrahedral bonding to phosphorus, and a 90° value for all *cis*-L–M–L bond angles was used. For chlorine at site 1 in **21a**, the *two P*-methyl carbons are each 3.0 Å away from the chlorine. A chlorine at site 2 is also 3.0 Å away from *four* proximate *tert*-butyl methyl carbons. For each of these $CH_3$/Cl interactions, the van der Waals radii of methyl and chlorine overlap by about 0.8 Å, which should be repulsive. Admittedly, the actual equilibrium geometries of **1** and **2** do not have $C_{2v}$ symmetry. Twisting about bonds and bond angle distortions will occur.[9-11] Nevertheless, it is apparent that the greater number of methyl groups proximate to site 2 in **21a** renders site 2 more crowded than site 1. The smaller carbon monoxide should prefer to locate at site 2 and the larger chlorine at site 1. Thus, we assign the major syn form of **1** or **2** to **17** (eq 1). The major $B_2X$ and $B_2$ signals in the $^{31}P\{^1H\}$ spectra of **1** and **2** at about 210 K (Table I) are assigned to **17** and the minor $D_2X$ and $D_2$ signals to **18**.

In an anti form, the larger chlorine ligand will experience *three* $CH_3$/Cl nonbonded repulsions, which should render the anti forms intermediate in stability between the two syn conformations. Indeed, this is observed (Table I).

(17) The carbon monoxide ligand was treated, to a first approximation, as a cylinder with a length (*l*), radius (*r*) and volume (*V*). The length (*l*) was derived from available C≡O bond length and van der Waals radii for carbon and oxygen and the volume from the work of Bondi.[18] With the dimensions thus set, the equation for the volume of a cylinder was solved for $r$ = 1.4 Å.

(18) (a) Bondi, A. *J. Phys. Chem.* **1964**, *68*, 441. (b) Slater, J. C. *J. Chem. Phys.* **1964**, *41*, 3199.

(19) Stevenson, P. E.; Merrill, J. E. Quantum Chemistry Program Exchange, Indiana University; Program 186.

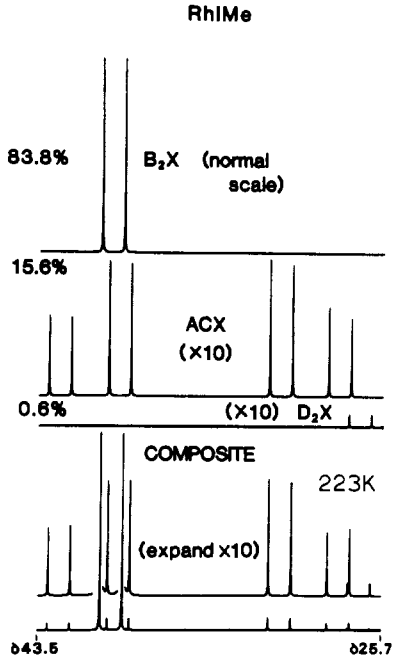


**Figure 10.** Decomposition of the $^{31}P\{^1H\}$ NMR spectrum of **4** at 223 K.

Now that these assignments have been made, certain structural variations should produce predictable changes in conformer populations. Specifically, increasing the steric size of halogen should enhance the relative stability of conformer **17** and decrease the relative stabilities of **18–20**. In addition, changing the $PCH_3$ groups to PH moieties should enhance the difference between the degrees of crowding at sites 1 and 2 in **21b** as compared to the case for **21a**. In **21b** site 1 should be substantially less crowded than site 1 in **21a**, while site 2 remains essentially unchanged. Larger halogen ligands will be much better accommodated at site 1 in **21b**. Thus, changing $PCH_3$ to PH groups should also enhance the relative stability of **17** as compared to **18–20**.

**Effect of Halogen Steric Bulk on Conformational Preference.** ***trans*-[$(t$-$C_4H_9)_2PCH_3]_2$Rh(CO)Br (3).** The $^{31}P\{^1H\}$ NMR spectrum (101.2 MHz) of the bromo complex **3** (0.03 M in toluene-$d_8$) at 370 K is a broadened doublet at $\delta$ 36.9 ($^1J_{RhP}$ = 120 Hz). Below 370 K, the spectrum decoalesces and, at 214 K, is sharpened into three subspectra (see Figure 7, supplementary material). A decomposition of the 214 K spectrum (see Figure 8, supplementary material) shows a major $B_2X$ doublet (**17**; 66.6%), a minor $D_2X$ doublet (**18**; 3.4%) and an ACX subspectrum (**19** and **20**; 30.0%). NMR parameters are compiled in Table I. This DNMR behavior is analogous to that for **1** but with important differences in subspectral populations. As compared to the case for **1**, the population of **17** has *increased* by 6.7% while the populations of **18** as well as **19** and **20** have *decreased* by 3.6% and 3.1%, respectively (Table I). The relative stability of conformer **17** has increased while the stabilities of **18–20** have decreased, as expected.

***trans*-[$(t$-$C_4H_9)_2PCH_3]_2$Rh(CO)I (4).** The $^{31}P\{^1H\}$ NMR spectrum of **4** shows a characteristic decoalescence (see Figure 9, supplementary material). A decomposition of the slow-exchange spectrum at 223 K (Figure 10) shows the typical $B_2X$ (**17**; 83.8%), $D_2X$ (**18**; 0.6%), and ACX (**19** and **20**; 15.6%) subspectra (Table I). In Figure 10, those spectra marked ×10 are displayed at an amplification 10 times larger than the $B_2X$ subspectrum and the bottom composite spectrum. As compared to the case for the bromo complex **3**, there is another significant increase in the relative population of conformer **17** (+17.2%) and decreases for **18** (−2.8%) as well as **19** and **20** (−14.4%), as expected.

***trans*-[$(C_4H_9)_2PCH_3]_2$Ir(CO)Br (5).** The $^{31}P\{^1H\}$ NMR spectrum of **5** (0.03 M in toluene-$d_8$) at 375 K shows a highly exchange-broadened signal at $\delta$ 31.5 (see Figure 11, supplementary material). The degree of exchange broadening for **5** at 375 K is substantially greater than for **2** at 360 K (Figure 4). This is consistent with higher rotation barriers due to a sterically larger

bromine. At 214 K, the spectrum is separated into $B_2$ (**17**; 70.5%), $D_2$ (**18**; 3.2%), and AC (**19** and **20**; 26.3%) subspectra (see Figure 12, supplementary material; Table I). As compared to the case for the chloro analogue (**2**), there is an increase in the relative population of **17** (+9.8%) and corresponding decreases for **18** (−3.1%) as well as **19** and **20** (−6.7%).

***trans*-[$(t$-$C_4H_9)_2PCH_3]_2Ir(CO)I$ (6).** The $^{31}P\{^1H\}$ spectrum of **6** (0.03 M in toluene-$d_8$) at 310 K already shows a substantially decoalesced spectrum (Figure 13, supplementary material). This reveals higher rotation barriers about Ir–P bonds than in the chloro analogue and a sterically larger iodine. The 242 K slow-exchange spectrum shows major $B_2$ (**17**; 84.5%), *very minor* $D_2$ (**18**; 0.6%), and AC (**19** and **20**; 14.9%) subspectra (Figure 14, supplementary material).

At this point, it should be stated that complete DNMR line-shape analyses for iodo complexes **4** and **6** show that the minor $D_2X$ or $D_2$ signals observed at low temperature do indeed coalesce with the rest of the spectrum at higher temperatures. The $D_2X$ and $D_2$ signals are not due to minor impurities and are due to molecular conformations associated with *intra*molecular exchange in **4** and **6**.

A perusal of Table I reveals a clear-cut trend. As the van der Waals radius and cone angle of halogen increases, the relative stability of **17** increases while the stabilities of **18** **19**, and **20** decrease. This is consistent with increasing steric bulk in proceeding from chlorine to bromine to iodine and an increasing differential between repulsions experienced by halogen at sites 1 and 2 in **21a**. As halogen steric bulk increases, there is a progressively greater preference for halogen to locate at the less sterically crowded site 1 in **21a** than at site 2 and an increasing preference for conformation **17**. Likewise, as halogen steric bulk increases, nonbonded methyl/halogen repulsions should increase in the anti forms **19** and **20**. The relative stabilities of **19** and **20** should decrease, as observed (Table I). These trends are entirely consistent with our conformational assignments.

**Effect of the P–R Group on Conformational Preference.** Consistent with our rationale for conformational assignments (vide supra), changing from P–$CH_3$ to P–H groups should enhance the relative stability of syn form **17** as compared to **18–20**.

***trans*-[$(t$-$C_4H_9)_2PH]_2Rh(CO)Cl$ (7).** The $^{31}P\{^1H\}$ NMR spectrum (101.2 MHz) of **7** (0.04 M in 20% $CDCl_3$/80% toluene-$d_8$) at 370 K shows an exchange-broadened resonance ($\delta$ 74.3), which decoalesces at lower temperatures into a familiar set of three subspectra (see Figures 15 and 16, supplementary material). NMR parameters are compiled in Table I. At 223 K, the spectrum shows $B_2X$ (**17** in eq 1; 78.2%), $D_2X$ (**18**; 1.0%), and ACX (**19** and **20**; 20.8%) subspectra.

One comparison is noteworthy. For **7**, the population of the dominant syn form **17** is substantially higher while minor syn and anti populations are lower than in the di-*tert*-butyl*methyl*phosphine analogue **1** (Table I). This is consistent with the fact that the larger halogen ligand can locate at the substantially less crowded site 1 in **21b** (as compared to site 1 in **21a**). This leads to an enhanced relative stability for conformer **17**.

***trans*-[$(t$-$C_4H_9)_2PH]_2Ir(CO)Cl$ (8).** The $^{31}P\{^1H\}$ spectrum (101.2 MHz) of **8** (0.03 M in $CDCl_3$) decoalesces in typical fashion (see Figure 17, supplementary material), revealing at 223 K dominant $B_2$ (**17**; 90.0%), AC (**19** and **20**; 9.8%), and *very minor* $D_2$ (**18**; 0.2%) subspectra (see Figure 18 (supplementary material) and Table I). For **8**, conformer **17** is once again more stable than for the methyl analogue **2**.

***trans*-[$(t$-$C_4H_9)_2PH]_2Rh(CO)Br$ (9) and *trans*-[$(t$-$C_4H_9)_2PH]_2Ir(CO)Br$ (10).** The $^{31}P\{^1H\}$ NMR spectra of **9** (0.03 M in $CDCl_3$) and **10** (0.03 M in $CDCl_3$) decoalesce in typical fashion. NMR parameters and subspectral populations are compiled in Table I. As expected, the relative stability of **17** has increased for **9** and **10** as compared to that for the chloro complexes **7** and **8**. For **9** and **10**, the minor syn conformer is present at minuscule concentrations (0.1–0.3%).

***trans*-[$(t$-$C_4H_9)_2PH]_2Rh(CO)I$ (11)** and ***trans*-[$(t$-$C_4H_9)_2PH]_2Ir(CO)I$ (12).** The $^{31}P\{^1H\}$ NMR spectra of **11** (0.03 M in $CDCl_3$) and **12** (0.03 M in toluene-$d_8$) also decoalesce in typical fashion. For **11** at 214 K, there is a strongly dominant $B_2X$ doublet (**17**; 93.5%) and an ACX subspectrum (**19** and **20**; 6.5%). *Even after many hours of signal averaging, we could detect no $D_2X$ subspectrum.* For **12** at 214 K, there is an even more strongly dominant $B_2$ singlet (**17**; 97.5%) and an AC subspectrum (**19** and **20**; 2.5%). We could detect no $D_2$ singlet. NMR parameters and subspectral populations are compiled in Table I. *For* **11** *and* **12**, *the minor syn species* (**18**; *eq 1*) *is present in too low a concentration to be NMR detectable, and syn form* **17** *is strongly dominant.*

**Trends in Conformational Preference.** The consistency between our rationale for conformational assignments and the trends in conformational preference determined from the $^{31}P\{^1H\}$ NMR data (vide supra) strongly suggest conformer **17** to be the most stable equilibrium conformation.

For both series of complexes (**1–6**, **7–12**), proceeding from iodine to bromine to chlorine corresponds to a reduction in steric size for halogen that is progressively more comparable to carbon monoxide. The differential between methyl/halogen and methyl/carbon monoxide repulsions should progressively decrease with decreasing halogen van der Waals radius and the population differences between conformers should also decrease, as observed (Table I). The relative stabilities of the minor syn form **18** and anti forms (**19**, **20**) progressively *increase* as halogen size *decreases*.

Comparisons between pertinent pairs of the two series **1–6** and **7–12** (Table I) will also show that changing from R = H to R = $CH_3$ results in a *destabilization* of the major syn conformer (**17**) and increased relative stabilities for **18–20**. This trend is consistent with the fact that the *difference* between nonbonded repulsions felt by halogen at sites 1 and 2 in **21a** is smaller than in **21b**. Steric crowding at site 1 in **21a** is more severe than it is in **21b**. The net result is a trend toward equalizing conformer populations in the *P*-methyl analogues.

**$^{31}P\{^1H\}$ Chemical Shift Trends.** Now that the conformational assignments above have been made, some potentially useful trends in $^{31}P\{^1H\}$ chemical shifts can be deduced as follows: (1) The chemical shift of the major syn species (**17**) with the P–R groups syn to halogen is in the higher frequency (downfield) region of the spectrum (Table I). (2) The chemical shift of the minor syn species (**18**) with the P–R groups syn to carbon monoxide is in the lower frequency (upfield) region of the spectrum. (3) For the anti species, the higher frequency signal is due to the P–R group that is syn to halogen and the lower frequency signal is due to the P–R group that is syn to carbon monoxide.

**Dynamics of Rotation about Metal–Phosphorus Bonds.** A $^{31}P\{^1H\}$ NMR line-shape simulation model for complexes **1–8** requires the incorporation of *four* unique spin systems: $B_2X$ (or $B_2$), $D_2X$ (or $D_2$), ACX (or AC), and CAX (or CA).[20] While the two anti forms **19** and **20** are equivalent, they can be interconverted *directly* by simultaneous 180° rotations of *both* phosphines about the M–P bonds. During this process, the two diastereotopic phosphorus atoms interchange chemical shifts (i.e., ACX to CAX or AC to CA). Therefore, the *direct* anti to anti conversion (e.g., **19** to **20**) is in principle a DNMR-visible process, as are all the other possible conformational exchanges shown in eq 1. A general equation that catalogues all possible subspectral exchanges for complexes **1–8** is shown in eq 2. Equation 2

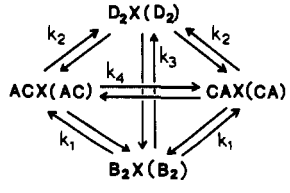


(2)

correlates directly to eq 1 in terms of spin systems, the conformational assignments made above, and rate constants. Six rate constants are shown in eq 1 and 2. The corresponding reverse rate constants are all implied and are automatically calculated

(20) DNMR simulations were not performed for complexes **9–12**.

**Table IV.** Activation Parameters for Rotation about the Metal–Phosphorus Bonds in Complexes **1–8**

| compd | spin exchange obsd | $\Delta H^{\ddagger}$, kcal/mol | $\Delta S^{\ddagger}$, cal/mol-deg | $\Delta G^{\ddagger}$, kcal/mol (temp, K) |
|---|---|---|---|---|
| **1** | $B_2X$ to ACX | 12.9 ± 1.5 | −2 ± 7 | 13.4 ± 0.2 (266) |
| | ACX to $D_2X$ | 11.9 ± 1.5 | −3 ± 7 | 12.7 ± 0.2 (266) |
| **2** | $B_2$ to AC | 14.4 ± 1.5 | 2 ± 7 | 13.9 ± 0.2 (271) |
| | AC to $D_2$ | 12.2 ± 1.5 | −5 ± 7 | 13.5 ± 0.2 (271) |
| **3** | $B_2X$ to ACX | 13.1 ± 1.5 | −4 ± 7 | 14.1 ± 0.2 (271) |
| | ACX to $D_2X$ | 12.9 ± 1.5 | −4 ± 7 | 13.9 ± 0.2 (271) |
| **4** | $B_2X$ to ACX | 11.8 ± 1.5 | −10 ± 7 | 14.7 ± 0.2 (290) |
| | ACX to $D_2X$ | 12.2 ± 1.5 | −7 ± 7 | 14.4 ± 0.2 (290) |
| **5** | $B_2$ to AC | 13.3 ± 1.5 | −6 ± 7 | 15.2 ± 0.2 (300) |
| | AC to $D_2$ | 13.6 ± 1.5 | −4 ± 7 | 14.9 ± 0.2 (300) |
| **6** | $B_2$ to AC | 16.0 ± 1.5 | 1 ± 7 | 15.8 ± 0.2 (300) |
| | AC to $D_2$ | 14.5 ± 1.5 | −3 ± 7 | 15.4 ± 0.2 (300) |
| **7** | $B_2X$ to ACX | 11.4 ± 1.5 | −7 ± 7 | 13.5 ± 0.2 (271) |
| | ACX to $D_2X$ | 11.1 ± 1.5 | −7 ± 7 | 13.1 ± 0.2 (271) |
| **8** | $B_2$ to AC | 12.0 ± 1.5 | −8 ± 7 | 14.2 ± 0.2 (280) |
| | AC to $D_2$ | 11.5 ± 1.5 | −8 ± 7 | 13.9 ± 0.2 (280) |

in the DNMR line-shape calculations.[13]

The $^{31}P\{^1H\}$ DNMR spectra of **1–8** decoalesce above 200 K due to slowing rotation about M–P bonds. Excellent line-shape simulations were achieved with $k_3$ and $k_4$ values in eq 2 equal to zero and non-zero values for $k_1$ and $k_2$. Incorporation of $k_3$ or $k_4$ values that were above 10% of the other rate constants produced subtle but discernible degradations in the DNMR line-shape simulations.

Although the error in temperature measurement at the NMR sample is ±3 K, decoalescence generally occurs over a *large temperature range* (ca. 120 K) and we feel justified in reporting $\Delta H^{\ddagger}$, $\Delta S^{\ddagger}$, and $\Delta G^{\ddagger}$ values for M–P rotation from least-squares fits of Eyring plots (Table IV). Of course, $\Delta G^{\ddagger}$ values must be considered to be the most accurate of the three activation parameters.

There are implications to be derived from the DNMR simulations. The requirement that $k_3$ and $k_4$ values equal zero says the *direct* syn to syn (e.g., **17** and **18**) and *direct* anti to anti (**19** to **20**) conversions occur at rates that are slower than syn to anti exchanges. The preferred itinerary for exchange involves stepwise interconversions around the periphery of eq 1 or 2. One phosphine at a time rotates 180°, presumably passing through two maxima involving *t*-$C_4H_9$/halogen and *t*-$C_4H_9$/CO eclipsings and via an unstable intermediate (e.g., see **16**). The DNMR simulations show that M–P rotation barriers do increase with increasing steric size of halogen and the barriers in the iridium complexes are slightly higher than in the rhodium complexes (Table IV).

## Experimental Section

The 101.2-MHz $^{31}P\{^1H\}$ and 62.9-MHz $^{13}C\{^1H\}$ NMR spectra were recorded with use of a Bruker WM-250 NMR system at the University of Vermont. The 67.9-MHz $^{13}C\{^1H\}$ spectra were recorded on a Bruker HX-270 NMR system at the NSF Regional Instrumentation Center at Yale University. Variation of NMR sample temperature was achieved with use of a custom-built nitrogen gas delivery system, and temperature was controlled with a Bruker BVT-1000 control unit. Temperatures could be maintained at a constant value (±0.1 K) but are accurate to only ±3 K at the sample. NMR samples were prepared in precision NMR tubes on a vacuum line and were sealed after a minimum of three freeze/pump/thaw cycles (0.01 torr).

Mass spectral analyses were provided by the Analytical Section of Warner-Lambert/Parke-Davis Pharmaceuticals, Ann Arbor, MI. Mass measurements were made by using a high-resolution VG7070 E/HF mass spectrometer operating in either the fast atom bombardment (FAB) or desorption electron ionization (DEI) mode. For the FAB experiments, the matrix used is thioglycerol and the reagent gas used is xenon.

Syntheses of complexes **1**, **2**, **7**, and **8** have been described previously.[5b]

***trans*-[(*t*-$C_4H_9$)$_2$$PCH_3$]$_2$Rh(CO)Br (3)** was prepared from **1** by six separate treatments with a stirred 6 M excess of lithium bromide in methanol at reflux for 24 h. After each exchange, the mixture was cooled to 273 K and the precipitated complex isolated by filtration. Examination of the $^{31}P\{^1H\}$ and $^{13}C\{^1H\}$ NMR spectra after each exchange showed a smooth and eventually complete conversion to **3**. Following the last exchange, **3** was washed with methanol and recrystallized from 50% toluene/50% methanol. NMR data: Table I. Mass spectral data: *m/e* 530 (FAB); calcd $M_r$, 531.4. Anal. Calcd for $C_{19}H_{42}BrOP_2Rh$: C, 42.9; H, 7.97; P, 11.7; Br, 15.0. Found: C, 43.1; H, 7.92; P, 11.5; Br, 14.7.

***trans*-[(*t*-$C_4H_9$)$_2$$PCH_3$]$_2$Rh(CO)I (4)** was prepared from **1** with use of sodium iodide and the procedure described for **3** above. NMR data: Table I. Mass spectral data: *m/e* 578 (FAB); calcd $M_r$, 578.4. Anal. Calcd for $C_{19}H_{42}IOP_2Rh$: C, 39.5; H, 7.32; P, 10.7; I, 21.9. Found: C, 39.4; H, 7.36; P, 10.2; I, 21.0.

***trans*-[(*t*-$C_4H_9$)$_2$$PCH_3$]$_2$Ir(CO)Br (5)** was prepared from **2** with use of lithium bromide and the proedure described for **3** above. NMR data: Table I. Mass spectral data: *m/e* 620 (FAB); calcd $M_r$, 620.6. Anal. Calcd for $C_{19}H_{42}BrOP_2Ir$: C, 36.8; H, 6.82; P, 10.0; Br, 12.9. Found: C, 36.0; H, 6.82; P, 9.42; Br, 12.0.

***trans*-[(*t*-$C_4H_9$)$_2$$PCH_3$]$_2$Ir(CO)I (6)** was prepared from **2** with use of sodium iodide and the procedure described for **3** above. NMR data: Table I. Mass spectral data: *m/e* 668 (FAB); calcd $M_r$, 667.6. Anal. Calcd for $C_{19}H_{42}IOP_2Ir$: C, 34.2; H, 6.34; P, 9.28; I, 19.0. Found: C, 34.2; H, 6.44; P, 9.07; I, 18.7.

***trans*-[(*t*-$C_4H_9P$)$_2$$PH$]$_2$Rh(CO)Br (9)** was prepared from **7** with use of lithium bromide and the procedure described for **3** above. NMR data: Table I. Mass spectral data: *m/e* 502 (DEI); calcd $M_r$, 503.2. Anal. Calcd for $C_{17}H_{38}BrOP_2Rh$: C, 40.6; H, 7.61; P, 12.3; Br, 15.9. Found: C, 40.7; H, 7.70; P, 11.7; Br, 14.5. A persistent trace of starting material (**7**) is observed in the $^{31}P\{^1H\}$ NMR spectrum and the sample did give an analysis for some chlorine (1.25%).

***trans*-[(*t*-$C_4H_9$)$_2$$PH$]$_2$Ir(CO)Br (10)** was prepared from **8** with use of lithium bromide and the procedure described for **3**. NMR data: Table I. Mass spectral data: *m/e* 592 (DEI); calcd $M_r$, 592.5. Anal. Calcd for $C_{17}H_{38}BrOP_2Ir$: C, 34.5; H, 6.46; P, 10.5; Br, 13.5. Found: C, 35.6; H, 6.80; P, 9.29; Br, 12.3. A persistent trace of starting material (**8**) is observed in the $^{31}P\{^1H\}$ NMR spectrum and the sample did give an analysis for some chlorine (0.95%).

***trans*-[(*t*-$C_4H_9$)$_2$$PH$]$_2$Rh(CO)I (11)** was prepared from **7** with use of sodium iodide and the procedure described for **3** above. NMR data: Table I. Mass spectral data: *m/e* 550 (DEI); calcd $M_r$, 550.2. Anal. Calcd for $C_{17}H_{38}IOP_2Rh$: C, 37.11; H, 6.96; P, 11.3; I, 23.1. Found: C, 37.14; H, 7.03; P, 11.0; I, 22.8.

***trans*-[(*t*-$C_4H_9$)$_2$$PH$]$_2$Ir(CO)I (12)** was prepared from **8** with use of sodium iodide and the procedure described for **3** above. NMR data: Table I. Mass spectral data: *m/e* 640 (DEI); calcd $M_r$, 639.5. Anal. Calcd for $C_{17}H_{38}IOP_2Ir$: C, 31.93; H, 5.99; P, 9.69; I, 19.84. Found: C, 31.97; H, 6.01; P, 9.59; I, 19.5.

**Acknowledgment.** We are grateful to the National Science Foundation for financial support (Grant Nos. CHE-8024931 and CHE-8306876) and to the University of Vermont Academic Computing Center for outstanding computational support. We are also grateful to Steve Werness and Dana DeJohn of Warner-Lambert/Parke-Davis Pharmaceuticals for running the mass spectra.

**Registry No.** **1**, 34365-67-8; **2**, 34365-68-9; **3**, 101403-82-1; **4**, 101403-83-2; **5**, 101403-84-3; **6**, 101403-85-4; **7**, 33246-87-6; **8**, 33246-91-2; **9**, 33246-88-7; **10**, 33246-92-3; **11**, 33246-89-8; **12**, 33246-93-4.

**Supplementary Material Available:** $^{31}P\{^1H\}$ and $^{13}C\{^1H\}$ DNMR spectra of complexes **2–8** and decompositions of slow-exchange $^{31}P\{^1H\}$ NMR spectra for complexes **2**, **3**, and **5–8** (Figures 4–9 and 11–18) (14 pages). Ordering information is given on any current masthead page.